Proceedings World Geothermal Congress 2020+1
Reykjavik, Iceland, April - October 2021

Aerial Thermal Infrared Survey of the Buranga Geothermal Prospect, Uganda

Mark Harvey[1], Godfrey Bahati[2], Edward Isabirye[2], William Cumming[4], Nicholas Hinz[5], David Sussman[6] and Thomas Askew[6]

[1]University of Connecticut, Storrs, USA

[2]Geothermal Resources Department, Ministry of Energy and Mineral Development, Entebbe, UGANDA

[4]Cumming Geoscience, Santa Rosa CA, USA

[5]Geologica Geothermal Group, Inc., San Francisco, USA

[6]UK Department of International Development East African Geothermal Energy Facility (EAGER)

Keywords: drone, UAV, thermal, infrared, hydrothermal, photogrammetry, energy, plant, survey, exploration

ABSTRACT

A drone-based aerial thermal infrared (TIR) and high resolution color imaging survey at the Buranga geothermal prospect in Uganda was completed in 2018 to facilitate safe access for exploration programs, constrain structure and shallow aquifer mapping, support heat flow estimates and provide environmental baseline imaging. About 2000 thermal images were captured by a drone over a period of 3 days and compiled to produce a 0.8 km^2 georeferenced, temperature-calibrated thermal orthophoto map with a pixel width of about 13 cm and positional error under 3.5 m. The complementary visible light color orthophoto map had a pixel width of 2.5 cm. High-resolution imaging was required for the survey because the wetland vegetation of Buranga would otherwise obscure the numerous small hot spring vents that are characteristic of the prospect. The TIR imaging was correlated with over 75 shallow temperature measurements made with ground probes in order to validate the completeness of the ground mapping and support the interpretation of the TIR imaging with respect to temperatures 10 to 30 cm below the ground surface or in mud below shallow water. The TIR confirmed that the ground probe surveys had been thorough in mapping the area of the 75 vents but had missed a few thermal features separated from the main vent clusters and obscured by vegetation or shallow water. This extended the area affected by the shallow hot aquifers at Buranga.

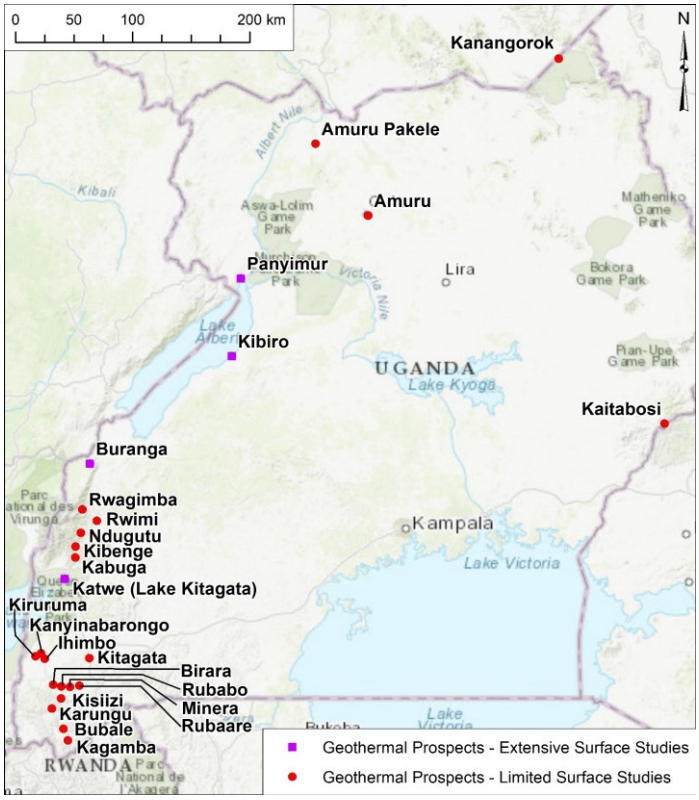

Figure 1: Buranga location relative to all 25 known geothermal prospects in Uganda.

1. INTRODUCTION

The Buranga geothermal prospect is located in the Albertine rift in western Uganda (Figure 1). Previous studies (e.g., Gislason, 1994; EAGER, 2017) have identified numerous near-boiling and boiling springs, but vegetation and swampy ground have limited the ability to complete comprehensive mapping of the surface manifestations. Comprehensive mapping of the thermal features is needed to update and establish confidence in exploration models, plan safe and effective geophysical studies, or target wells. To

address the challenges and help complete the surface studies that have previously been initiated only by foot, an Unmanned Aircraft System (UAS) survey was designed and conducted to provide high resolution thermal infrared (TIR) and red-green-blue (RGB) orthophoto imagery.

2. EXPLORATION HISTORY

Descriptions of Buranga Hot Springs were first published in the 1920s and 1930s and these reports and papers are summarized in Gislason (1994). Numerous warm to boiling point hot springs were noted to cover an area of more than >100 m^2. Three of the larger flow rate springs along the NW side are associated with travertine mounds and are named, from northeast to southwest, Mumbuga (Female), Nyansimbe (Male), and Kagoro (Figure 2).

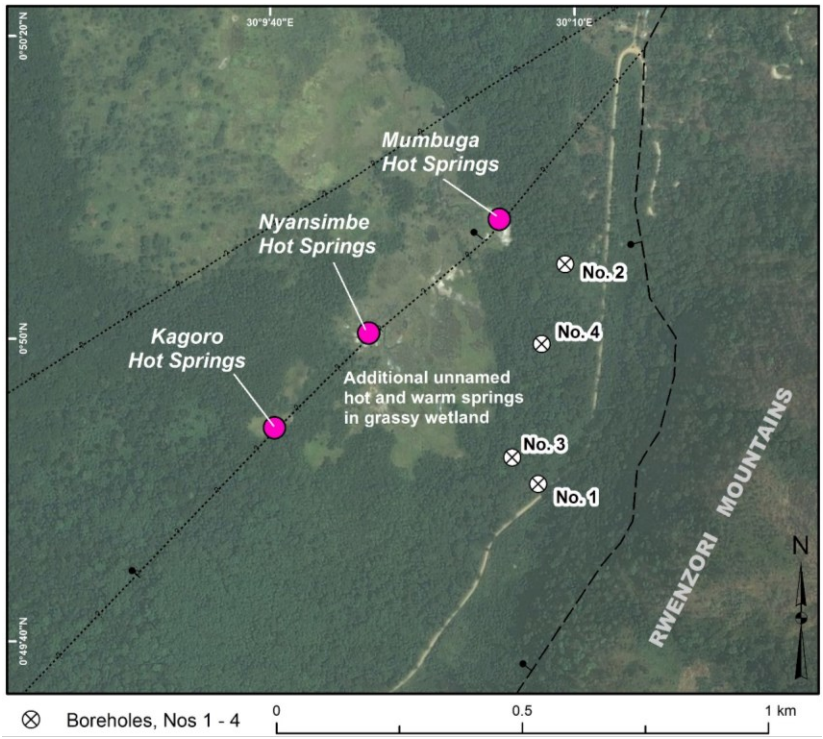

Figure 2: Historic hot spring names and 1950s drill holes (EAGER, 2017).

Formal geothermal exploration at Buranga began in the 1950s with geologic mapping, geophysical surveys, and drilling wells (Pallister, 1952; Brown, 1953; McConnell and Brown, 1954; also summarized in Gislason, 1994). In 1953-1954, attempts were made to drill four shallow wells near the thermal features at Buranga, and three holes were completed to depths ranging from 120 to 394 m. These holes established a dip measurement on the basin-bounding fault of 64° based on the distance to the surface trace of the fault, identified permeable zones in the basin fill sediments and some wells recorded near-boiling temperatures (Gislason, 1994).

Multiple geochemistry studies have been conducted at Buranga (e.g., Sharma, 1971; Bahati 1993; Armannsson et al., 2007). BGR and GSMD conducted a multidisciplinary study that included earthquake tomography, gravity, geochemistry, structural analysis via remote sensing, and a self-potential/resistivity study (e.g. Ochmann et al., 2007). In 2015, an MT-TEM survey was completed by GDC of Kenya on behalf of the private concession holder GIDS-Consult, with some results abstracted in Natukunda and Bahati (2015). In 2016, EAGER assisted GRD in a 26 MT station training survey on the south perimeter of the concession. In 2017, GRD acquired 17 additional MT stations to fill gaps in the MT coverage around the periphery of the Buranga Hot Spring area. However, none of these geophysical surveys effectively constrained the resource conceptual model because they lacked sufficient coverage within about 1 km of the hot springs where access was limited by the swamp.

In September 2017, EAGER and GRD conducted field mapping of the hot springs by foot. During this field campaign, more than 75 hot springs, covering a triangular shaped area 0.5 km wide east-west, and 0.5 km wide north-south, for a total area of 0.125 km^2 (Figure 3). Hot spring pools range from 10 cm to several meters across, with most < 1 meter across. Pool depths range from a few cm to a couple meters. Of these hot springs, five separate clusters of hot springs measured >90°C. These include the cluster of hot springs at Mumbuga, and one hot spring at Kagoro. Also three other unnamed hot springs southeast of Nyansimbe, including the hottest spring at Buranga which is boiling vigorously at 98.7°C (temperature for boiling at about 670 m elevation above sea level). In addition to these higher temperature springs, 20 other intermediate-hot springs (between 70 and 90°C) were mapped during this field survey, and additional unmapped springs were observed in areas that could not be safely accessed due to deep near-boiling pools and/or dense vegetation.

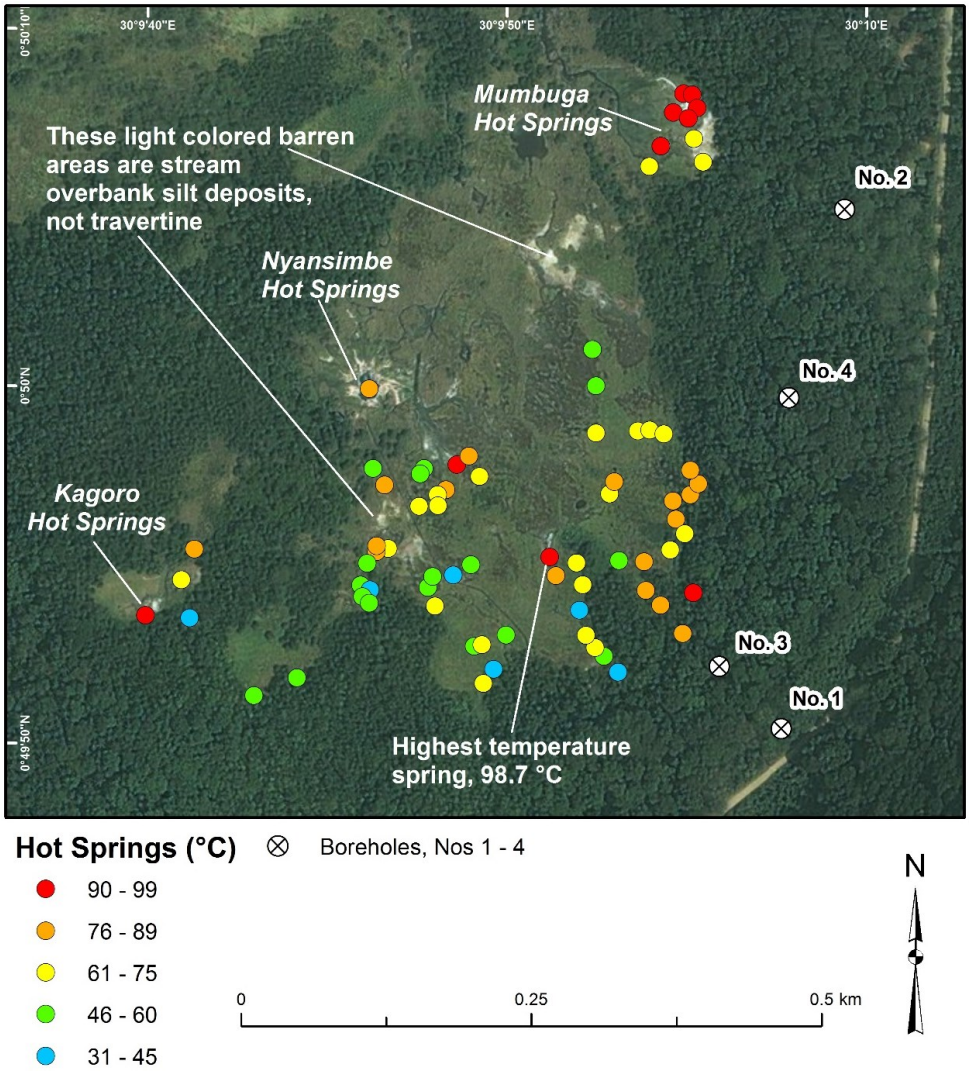

Figure 3: Map of active hot springs and existing drill holes at Buranga from EAGER (2017) using ESRI image base.

3. METHODOLOGY

For the UAS surveys, imagery was collected using a DJI Matrice 100 quadcopter (Figure 4). For TIR, the quadcopter was fitted with an ICI 640x480 uncooled TIR sensor (spectral response 7-14µm) with automated image capture. A Canon S100 point and shoot camera was fitted for normal visible (RGB) and DSM outputs.

To calibrate the georeferenced aerial data, 15 ground control points (GCP) were established prior to flight by placing reflective markers throughout the planned survey area. These were made from 12-inch vinyl records covered with aluminum foil (Figure 5). The location of the GCP was recorded using a Trimble R1 handheld DGPS receiver. The accuracy of the DGPS was 3 – 4 m at Buranga. An appropriate flight plan was determined using UgCS software based on the target area of interest (Figure 6). The flight plan was then uploaded to the quadcopter's flight controller. Accordingly, both in-flight navigation and image capture were autonomous.

All flights were made at 100 - 110 m altitude above ground, at a speed of 6 m/s. TIR images were collected in the early morning (0700 – 0900) to maximize temperature contrast between geothermal and non-geothermal areas. Visible imagery was collected around midday for maximum light and image acuity.

Ground truthing of the TIR raw sensor values was by direct measurement of water on the ground using a type-K thermocouple temperature probe immediately after the TIR flight on the second day of the survey.

Two-dimensional TIR and RGB images were converted to three-dimensional point clouds using Agisoft Photoscan® commercial photogrammetry software, running on a Hewlett Packard laptop computer equipped with an i7 processor and 32 GB RAM. Processing provided georeferenced, TIR and RGB raster orthophotos, and a DSM.

TIR imagery was post-processed using QGIS opensource desktop GIS. This involved conversion of the raw TIR sensor values to calibrated temperature values (°C).

Figure 4: **DJI Matrice 100 quadcopter.**

Figure 5: GCP made from a 12" vinyl record covered with aluminium foil.

4. RESULTS

For the visible imagery and DSM, 3 flights were made between the 22nd and 24th February 2018. Flight conditions were partly cloudy, with a maximum wind speed of ~20 km/h. The total flight time was about 45 minutes, providing 1430 images. Computer post-processing of imagery took about 20 hours, providing 15 orthophoto tiles and DSM with a total coverage of 1.2 km^2, and orthophoto ground resolution of 2.5 cm (pixel width) (Figure 6 and Figure 7). The GCP allowed improved georeferencing of the orthophoto and gave an estimate of the positional error (x-axis 3.5 m, y-axis 2.0 m and z-axis 5.1 m). For TIR imagery, 6 flights were made between 22nd and 25th February 2018. Flight conditions were partly cloudy and mild (20 - 26°C), with a maximum wind speed of ~5 km/h (morning wind speed was lower than at midday). The total flight time was about 90 minutes, providing 2216 TIR images. Computer post-processing of imagery took about 5 hours, providing a single TIR orthophoto with a total coverage of 0.84 km^2 and ground resolution of 13.2 cm (Figure 8 and Figure 9).

Nearly all the target area of interest was mapped (both TIR and non-TIR imagery). Small gaps in the TIR orthophoto occur in areas of dense vegetation with uniform forest canopy temperature (i.e. very low image contrast). These areas probably do not contain significant surface thermal features; any significant thermal feature will create a clearing and be visible from the above. Manual cross-checking alignment of the TIR orthophoto with the visible orthophoto was undertaken at 20 evenly distributed check points. This provided positional error for the TIR orthophoto relative to the RGB orthophoto (average offset of 2.5 m). A localised offset (~6 m) occurs along the warm outflow that drains both major hot springs and extends to the north.

Figure 9 shows an enlargement of the Nyansimbe Hot Spring area and illustrates both i) image quality, and ii) the improvement of TIR mapping over ground-based surveying approaches (points and polygons). Calibration of the TIR image showed a linear pixel response to surface temperatures directly measured through the thermocouple ground truthing exercise. A linear equation was fitted to the calibration scatter plot (Figure 10), which allows temperature to be estimated for each pixel (Figure 8, Figure 9). The calibrated TIR orthomosaic image is based on the linear equation.

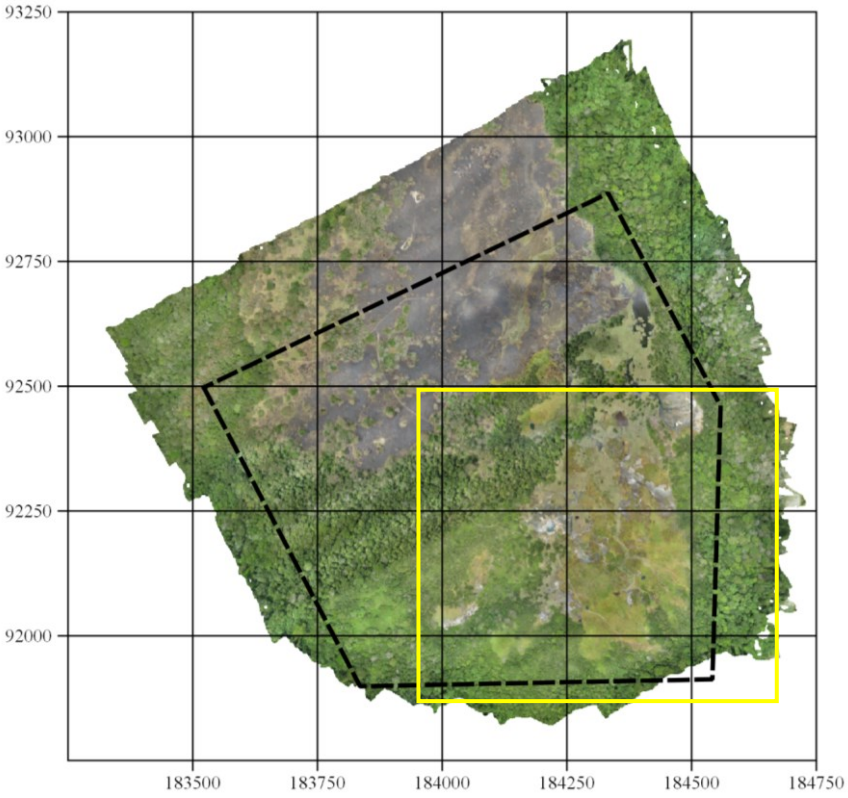

Figure 6: Visible orthophoto. Map Datum WGS84. Black dash line shows survey target area. Yellow square shows Figure 3 area. Note: two apparent NE-oriented bands of trees traversing the central part of the survey area may be an artifact of variable sunlight conditions during data collection.

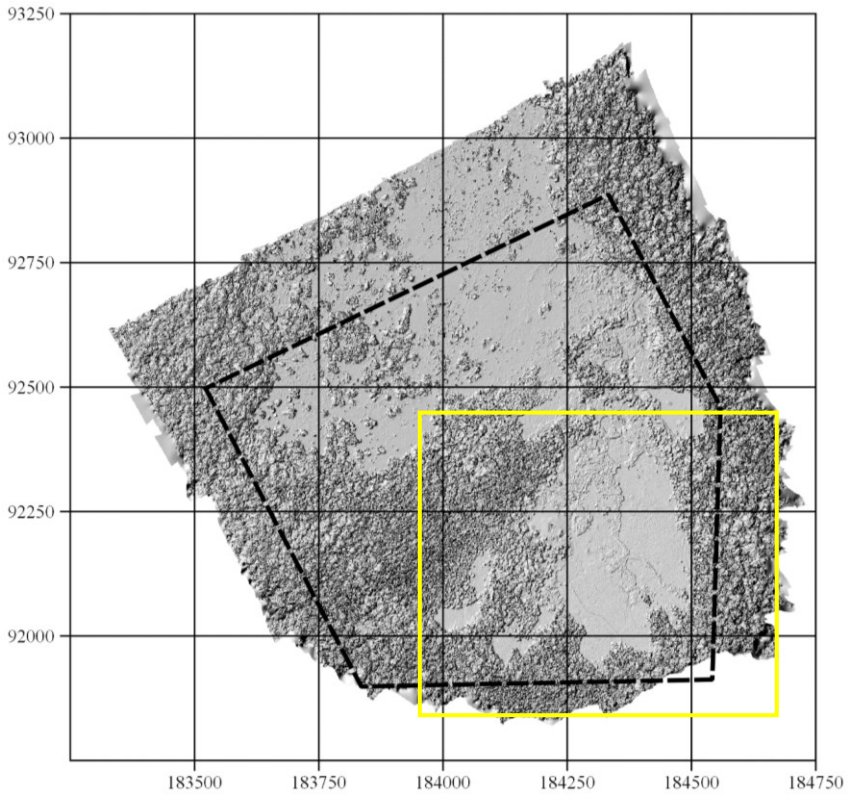

Figure 7: Digital surface model (DSM). Map Datum WGS84. Note: Black dash line shows survey target area. Yellow square shows Figure 3 area.

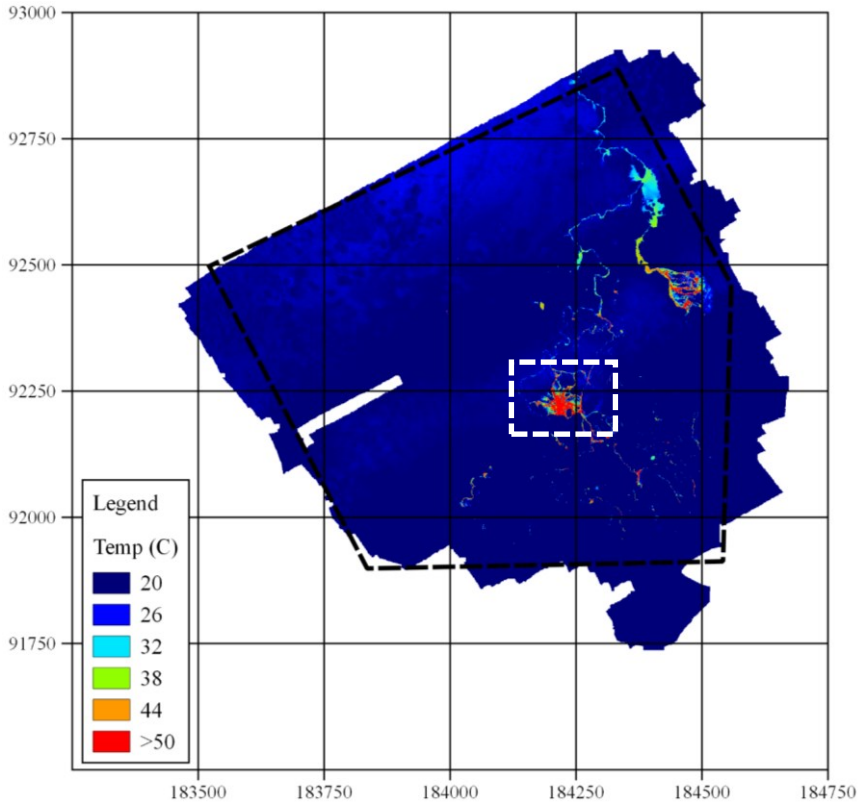

Figure 8: TIR orthophoto. Map Datum WGS84. Note: Black dash line shows survey target area, white dash box shows Nyansimbe Hot Spring detail area (Figure 9)

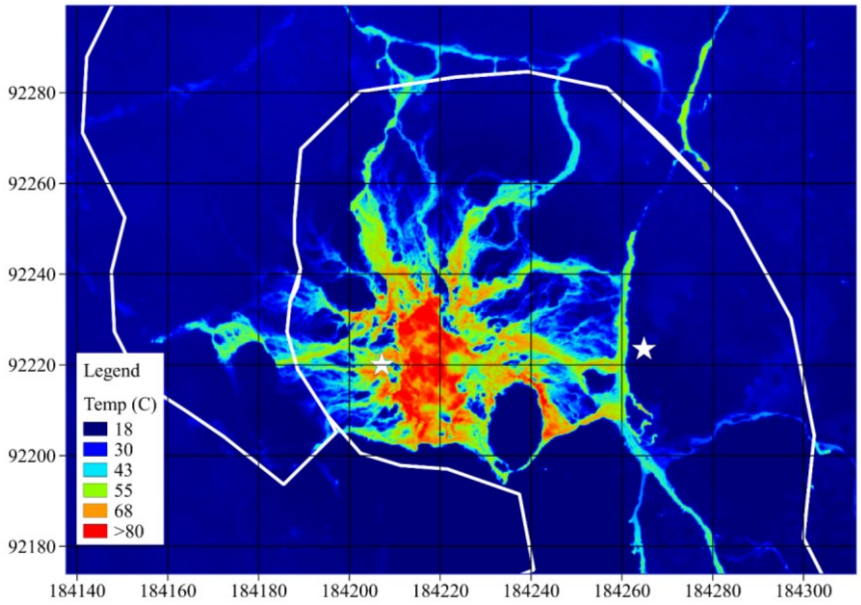

Figure 9: TIR orthophoto detail area (Nyansimbe Hot Spring - see white box in Figure 8) illustrating image quality. For comparison with previous ground-based surveying: solid white line shows mapped extent of geothermal hazards in the area, and white star shows previously mapped thermal features. Note: temperature scale has been expanded to provide contrast across a wider range of temperatures. Map Datum WGS84.

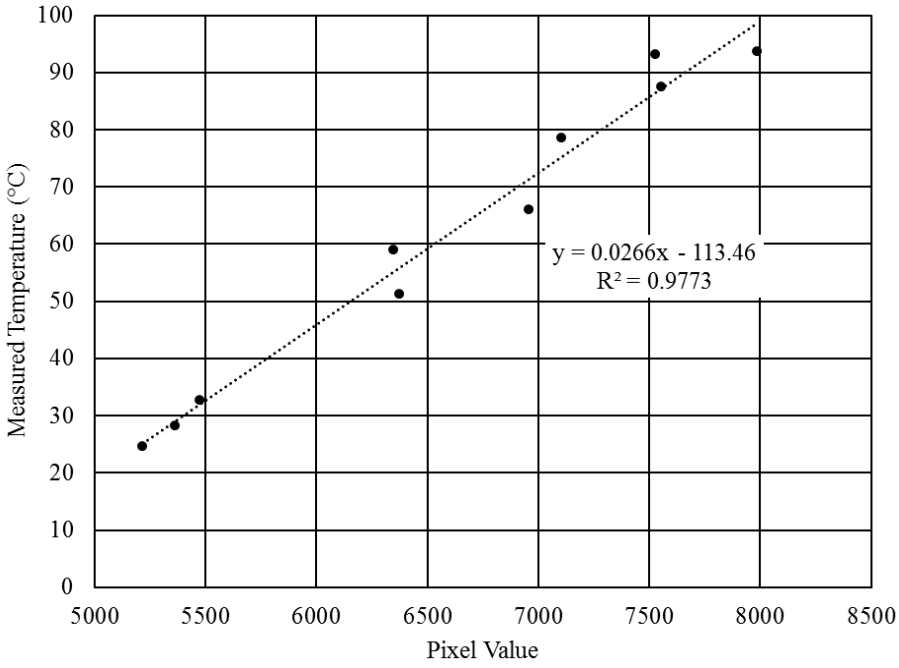

Figure 10: TIR camera calibration.

5. SUMMARY AND CONCLUSIONS

The most significant output of this study is the production of a 0.8 km^2 georeferenced, temperature-calibrated TIR orthophoto of the Buranga thermal area. The image represents a mosaic of about 2000 TIR images captured by UAS over a period of 3 days.

In summary:

- TIR imagery was calibrated by ground truthing; pools of various temperatures were measured with a thermocouple just after flying the survey. The correlation in the cross-plot is good ($r^2 = 0.98$), and calibrated temperatures are about ±3°C throughout much of the temperature range. This has allowed the delivery of calibrated and georeferenced TIR imagery that can be investigated in detail with standard GIS software (ArcGIS, QGIS, etc.).

- The assignment demonstrated clearly how high-quality maps and images can be obtained quickly and economically. The information will also make future ground surveys easier to plan and execute, and improve upon the quality of imagery available through satellites; the data is of significantly higher resolution compared with that currently available to GRD from satellite or other remote sensing techniques.

- Hot springs, pools, thermal ground, and various types of vegetation are clearly identifiable in TIR imagery. The locations, areal extent and temperature of geothermal surface features can now be more efficiently quantified (using GIS) compared to ground-based methods.

- Imagery enables the planning of safe access when undertaking surveys, especially involving heavy equipment.

The TIR data provides a detailed platform to compare against previous ground surveys. Overall, the resulting pattern confirms the triangular footprint previously established for the spring distribution. New springs were identified in the TIR imagery north of Nyansimbe that were previously unknown, and thus expanding the previously known footprint. Others were also identified around Nyansimbe, all of which were inaccessible on the ground due to near-boiling swampy ground. Future work should include comparison of all 75 previously measured spring points with the TIR data to evaluate specifically how many springs may have been missed in previous field studies, as well as the full range of variation in the temperature signal.

REFERENCES

Armannsson, H., Bahati, G., & Kato, V. (2007). Preliminary investigations of geothermal areas in Uganda, other than Katwe-Kikorongo, Buranga and Kibiro Final Report. *ICEIDA, MEMD, Uganda*.

Bahati, G. (1993). Geochemical Studies on Waters from the Katwe-Kikorongo, Buranga and Kibiro Geothermal Areas, Uganda. United Nations University.

Brown, J. M. (1953). Report on the Buranga hot springs: Uganda Geol. *Survey Rept. JMB/12*.

EAGER (2017). Buranga and Panyimur review and conceptual models: Confidential Presentation to GRD, December, 76 slides.

Gislason, G. (1994). *Geothermal Exploration-I*. UGA/92/002 & UGA/92E01. Terminal Report.

McConnell, R.B. & Brown, J.N. (1954). Drilling for geothermal power at Buranga Hot Springs, Toro. First Progress Report. Geological Survey of Uganda, Unpub. report No. JMB/17 (RBM/16).

Natukunda, J. F., & Bahati, G. (2015). The three geothermal prospects of Uganda: Kibiro, Katwe and Buranga–Geology and geothermal surface manifestations. In *Proceedings World Geothermal Congress*.

Ochmann, N., Lindenfeld, M., Barbirye, P., & Stadtler, C. (2007). Microearthquake survey at the Buranga geothermal prospect, western Uganda. In *Proceedings of Thirty-Second Workshop on Geothermal Reservoir Engineering* (pp. 22-24).

Pallister, J.W., (1952). Buranga hot springs, Toro, Uganda. Geol. Surv. and Mines, Uganda, unpubl. report, JWP/14, 12 pp.

Sharma, V. (1971). Report on the preliminary survey of thermal anomalies of Western Uganda for the possible development of Geothermal Energy, DGSM.